

Phase behavior and structure of star-polymer–colloid mixtures

J. Dzubiella,^{a)} C. N. Likos, and H. Löwen

Institut für Theoretische Physik II, Heinrich-Heine-Universität Düsseldorf, Universitätsstraße 1, D-40225 Düsseldorf, Germany

(Received 18 January 2002; accepted 8 March 2002)

We calculate the phase diagrams of mixtures between hard-sphere colloids and star-polymers of arm numbers $f=2,6,32$ for different star-polymer–colloid size ratios $0.2 \leq q \leq 0.6$ using an effective one-component description for the colloids in the presence of the stars. We map the full two-component system onto an effective one-component system by inverting numerically the Ornstein–Zernike equation for binary mixtures, supplemented by the Rogers–Young closure, in the low-colloid density limit. The free energy for the fluid and crystalline phase is calculated by using both hard-sphere perturbation theory and thermodynamic integration of simulation data. We find stable fluid–fluid demixing transitions for low arm numbers $f=2,6$ above a critical value of the size ratio q_c below preempted by a fcc-solid. For the linear polymer limit, $f=2$, the critical size ratio is found to be $q_c \approx 0.4$, in agreement with other approaches to colloid-polymer mixtures. Increasing the arm number, the region of stability of the demixing transition with respect to crystallization of the colloids shrinks, and q_c grows. A comparison between the one- and two-component descriptions that demonstrates the consistency between the two routes is also carried out. © 2002 American Institute of Physics. [DOI: 10.1063/1.1474578]

I. INTRODUCTION

Multicomponent mixtures display an enormously richer phase behavior than one-component systems. A typical pure substance consisting of spherically symmetric molecules without internal degrees of freedom, displays a generic phase behavior on the temperature-pressure plane that features three phases: a gaseous and a liquid one (if sufficiently strong attractions between the molecules are present) and a crystal.¹ Moreover, the Gibbs phase rule² asserts that there is only one point in the phase diagram at which these three can be found in simultaneous coexistence with one another. Consequently, investigations of the bulk thermodynamics of one-component systems focus on the calculation of the freezing- and liquid-gas coexistence curves, as well as on the properties in the neighborhood of the critical point associated with the latter. In multicomponent mixtures, the additional freedom provided by the flexibility of changing the concentration of any of the constituent species at will, opens up the possibility of various types of phase transitions, such as, e.g., vapor–liquid, demixing, crystallization of any of the number of the components, alloy formation, etc. Thereby, new topological features in the phase diagram, including regions of multiphase coexistence, lines of critical points and critical end points show up. It is therefore not much of a surprise that the structure and thermodynamics of multicomponent mixtures are studied in much less detail than those of pure substances.

In soft matter physics, on the other hand, mixtures are the rule, not the exception. To complicate matters even further, typical soft matter systems include components with a vast separation of length scales, a feature that makes a true,

multicomponent description of real systems unfeasible.³ One possibility is to consider *model* mixtures and two examples that have been intensively investigated in the recent past⁴ are mixtures of hard spheres (colloids) and free, nonadsorbing chains on the one hand,^{5,6} and the binary hard sphere mixture (BHS) of two species with a variable size ratio on the other.^{7–9} Many of the theoretical investigations of the colloid–polymer (CP) mixture have been based on an *effective, one-component* description of the hard colloids, for which an additional, attractive depletion potential is introduced after the polymer has been integrated out. This is the well-known Asakura–Oosawa (AO) model,^{10,11} in which the polymers are figured as penetrable spheres experiencing in addition a hard-sphere (HS) interaction with the colloids. A number of theoretical investigations on the AO model^{12–15} have revealed that the system displays a demixing transition that accompanies the freezing of the hard colloids. However, the former becomes *metastable* with respect to the latter¹⁴ for polymer-to-colloid size ratios $q \leq q_c \approx 0.45$. For size ratios $q > q_c$, the system displays three phases: a colloid-poor/polymer-rich and colloid-rich/polymer-poor fluid, as well as a solid phase, in which the colloids form a fcc-crystalline arrangement with the polymers diffusing in it. However, for $q < q_c$, a single, mixed fluid and a crystal phase exist. These findings are in semi-quantitative agreement with experimental results.¹⁶ In the BHS system, two-component simulations¹⁷ have shown that the demixing transition in the fluid phase is either metastable with respect to crystallization or it is completely absent, depending on the size ratio.¹⁸ We note that in all cases mentioned above, freezing refers to the large hard spheres only: the crystallization of both components and the associated formation of binary alloys takes place at size ratios close to unity and its investigation by theoretical methods is highly nontrivial.^{19–21}

^{a)}Electronic mail: joachim@thphy.uni-duesseldorf.de

A theoretical understanding of the (meta)stability of the demixing transition in two-component mixtures is provided by the *depletion potential* that effectively acts between the larger components of the mixture when the smaller ones are thermodynamically traced out.²² Depletion is caused by the fact that the small components have more free space available to them when two large particles are brought close to contact than when they are far apart. Hence, an entropic effective attraction appears between the colloids. The procedure of tracing out the small components facilitates the theoretical studies but it is subject to two strong constraints arising from the definition of the effective interaction,²² namely (i) the overall thermodynamics of the mixture must, evidently, remain invariant in switching from one description to the other and (ii) the correlation functions of the large component should also be the same in both descriptions.

The purpose of this paper is twofold: on the one hand, by examining mixtures of colloids with star-polymers of variable arm-number f , we provide a natural bridge between the CP-mixture (corresponding to linear chains, $f=1$ and $f=2$) and to the BHS (formally $f\rightarrow\infty$). To this end, we derive depletion potentials between the colloids that, depending on f , interpolate between interactions similar as in the AO-model and the BHS-depletion interaction.^{23,24} On the other hand, we systematically investigate the consistency between the one- and two-component descriptions, since our starting point are the three interaction potentials acting between the two components. We trace out the phase diagrams of the mixture for various combinations of star arm numbers f (also called *functionalities*) and star-colloid size ratios. We find that already above $f\cong 10$, the generic behavior of the BHS-model with an absence of a demixing transition is reached. A brief account of this work has already been published elsewhere.²⁵

The rest of the paper is organized as follows: In Sec. II we give a review of the two-component description of star-polymer–colloid mixtures. Different methods of mapping this onto an effective one-component system are discussed and compared in Sec. III. The resulting phase diagrams are presented in Sec. IV and a comparison between the two- and one-component descriptions in Sec. V. In Sec. VI we draw our conclusions, and in the Appendix we present some technical details regarding the calculation of the Gibbs free energy.

II. TWO-COMPONENT DESCRIPTION

We start with the description of the full two-component mixture of star-polymers and hard spherical colloids. The applied interactions and resulting structural quantities are input for the mapping onto an effective one-component system

TABLE I. The fit parameters Λ , κ , τ for the effective star–colloid interaction of Eq. (6) and the star–star interaction Eq. (5) obtained from molecular simulation.

f	$\Lambda(f)$	$\kappa\sigma_s$	$\tau\sigma_s$
2	0.46	0.58	1.03
6	0.34	0.73	1.14
32	0.24	0.84	...

in Sec. III. Concerning the fluid–fluid demixing transition, the full, two-component system has been solved in Ref. 26 using fluid-integral equations and Monte Carlo simulations. Good agreement with experimental measurements has been found there.

We consider a binary system with N_c colloidal spheres of diameter σ_c (radius R_c) and N_s star polymers, characterized by a diameter of gyration σ_g (radius of gyration R_g) and an arm number f . The total particle number is $N=N_c+N_s$. Let $q\equiv\sigma_g/\sigma_c$ be the size ratio and $\rho_c\equiv N_c/V$ and $\rho_s\equiv N_s/V$ the number densities of the colloids and stars, respectively. We now define the packing fractions,

$$\eta_c = \frac{\pi}{6} \rho_c \sigma_c^3 \quad (1)$$

of the colloids, and

$$\eta_s = \frac{\pi}{6} \rho_s \sigma_g^3 \quad (2)$$

of the stars in the volume V . We investigate the thermodynamics of the mixtures on the basis of pair potentials between the two mesoscopic components, having integrated out the monomer and solvent degrees of freedom. Thus, three pair potentials are used as inputs for theory or simulation. The colloid–colloid interaction at center-to-center distance r is taken to be that of hard spheres (HS),

$$V_{cc}(r) = \begin{cases} \infty & \text{for } r \leq \sigma_c; \\ 0 & \text{else.} \end{cases} \quad (3)$$

The pioneering work in deriving the effective interaction between two stars in a good solvent was performed by Witten and Pincus.²⁷ There, it was shown that the interaction diverges logarithmically with star–star separation r as $r\rightarrow 0$. A full expression, valid for arbitrary separation has been derived theoretically and verified by neutron scattering and molecular simulation, where the monomers were explicitly resolved.^{28,29} The star–star pair potential is given by an ultrasoft interaction which is logarithmic for close approaches and shows a Yukawa-type exponential decay at larger distances,^{28,30}

$$V_{ss}(r) = \frac{5}{18} k_B T f^{3/2} \begin{cases} -\ln\left(\frac{r}{\sigma_s}\right) + (1 + \sqrt{f}/2)^{-1} & \text{for } r \leq \sigma_s; \\ (1 + \sqrt{f}/2)^{-1} \left(\frac{\sigma_s}{r}\right) \exp\left[-\frac{\sqrt{f}(r - \sigma_s)}{2\sigma_s}\right] & \text{else,} \end{cases} \quad (4)$$

with k_B being Boltzmann's constant and T the absolute temperature. Computer simulations have shown²⁹ that the so-called corona-diameter σ_s remains fixed for all considered arm numbers f , being related to the diameter of gyration through $\sigma_s \approx 0.66\sigma_g$. The theoretical approach giving rise to Eq. (4) does not hold for arm numbers $f \leq 10$, because the Daoud–Cotton model of a star,³¹ on which the Yukawa form of the decay beyond overlaps is based, is not valid for small f . In these cases, the interaction inclines to a shorter-ranged decay for $r > \sigma_s$. This is consistent with approaches in which at the linear polymer limit a Gaussian behavior of the pair potential is predicted.^{32–34} Only the large distance decay of the star–star interaction is modified for small f ; its form at close approaches has to remain logarithmic.²⁷ Accordingly, the following star–star pair potential for arm numbers $f \leq 10$, replacing the Yukawa by a Gaussian decay, has been put forward,³⁵

$$V_{ss}(r) = \frac{5}{18} k_B T f^{3/2} \begin{cases} -\ln\left(\frac{r}{\sigma_s}\right) + \frac{1}{2\tau^2\sigma_s^2} & \text{for } r \leq \sigma_s; \\ \frac{1}{2\tau^2\sigma_s^2} \exp[-\tau^2(r^2 - \sigma_s^2)] & \text{else,} \end{cases} \quad (5)$$

where $\tau(f)$ is a free parameter of the order of $1/R_g$ and is

$$V_{sc}(r) = \Lambda k_B T f^{3/2} \frac{\sigma_c}{2r} \begin{cases} \infty & \text{for } r < \frac{\sigma_c}{2}; \\ \xi_2 - \ln\left(\frac{2z}{\sigma_s}\right) - \left(\frac{4z^2}{\sigma_s^2} - 1\right) \left(\xi_1 - \frac{1}{2}\right) & \text{for } \frac{\sigma_c}{2} \leq r < \frac{\sigma_s + \sigma_c}{2}; \\ \xi_2 [1 - \text{erf}(2\kappa z)] / [1 - \text{erf}(\kappa\sigma_s)] & \text{else,} \end{cases} \quad (6)$$

where $z = r - \sigma_c/2$ is the distance from the center of the star polymer to the surface of the colloid. The constants are

$$\xi_1 = (1 + 2\kappa^2\sigma_s^2)^{-1} \quad (7)$$

and

$$\xi_2 = \frac{\sqrt{\pi}\xi_1}{\kappa\sigma_s} \exp(\kappa^2\sigma_s^2) [1 - \text{erf}(\kappa\sigma_s)]. \quad (8)$$

In Eq. (6) above, $\Lambda(f)$ and $\kappa(f)$ are fit parameters, obtained from computer simulations where the force between an isolated star and a hard flat wall is calculated, see Refs. 26 and 35. κ is in order of $1/\sigma_g$, see the values in Table I, whereas geometrical arguments yield a limit $\Lambda_\infty = 5/36 \approx 0.14$ for very large f .

Access to the thermodynamics of the mixture is obtained by solving the Ornstein–Zernike (OZ) equations for binary mixtures using the two-component Rogers–Young (RY) closure. The RY form is reliable for the one component star polymer system⁴⁰ and shows a spinodal instability in highly asymmetric hard sphere mixtures.⁷ Let us give a brief outline regarding integral equation theories for multicomponent mixtures. Consider, in general, a ν -component liquid mixture, consisting of N_1, N_2, \dots, N_ν particles of species

obtained by fitting to computer simulation results, see Refs. 26 and 35 and Table I. Using $\tau\sigma_s(f=2) = 1.03$ we obtain for the second virial coefficient of polymer solutions the value $B_2/R_g^3 = 5.59$, in agreement with the estimate $5.5 < B_2/R_g^3 < 5.9$ from renormalization group and simulations.³⁴

Equations (5) and (4) above yield the correct behavior of the overall prefactor for small and large values of f , respectively. Equation (5) yields the prefactor 5/18 for $f=1$, in agreement with the prediction $(\gamma-1)/\nu$ of Witten and Pincus,²⁷ and for $f=2$ the value 0.786, which is very close to the exact value 0.8 calculated by means of renormalization group techniques by des Cloizeaux.³⁶ Moreover, von Ferber *et al.* have demonstrated³⁷ that it is in very good agreement with up to three-loop calculations for f as high as 6. Equation (4), on the other hand, satisfies the $f^{3/2}$ -scaling of the prefactor for high f -values.²⁷ Extensions to polydisperse star-polymers have been also worked out.³⁸

An analytic form for the star-polymer–colloid pair potential can be found by integrating the osmotic pressure of one star along the spherical surface of a colloid, following an idea put forward by Pincus.³⁹ This can be achieved for arbitrary curvatures of the colloid but the analytical result below is accurate for size ratios $q \leq 0.7$ and reads as³⁵

1, 2, ..., ν , respectively, enclosed in the macroscopic volume V . The partial density ρ_i of species i , is given by $\rho_i = N_i/V$. The pair structure of the system is fully described by $\nu(\nu+1)/2$ independent correlation functions $h_{ij}(r)$, $i \leq j = 1, 2, \dots, \nu$, because symmetry with respect to exchange of the indices dictates $h_{ij}(r) = h_{ji}(r)$. Associated with the total correlation functions are the direct correlation functions (dcf's) $c_{ij}(r)$. For the same reasons, there exist only $\nu(\nu+1)/2$ independent dcf's. The Fourier transforms of $h_{ij}(r)$ and $c_{ij}(r)$ are denoted by $\tilde{h}_{ij}(k)$ and $\tilde{c}_{ij}(k)$, respectively.

The OZ relation for one-component systems at density ρ takes in Fourier space the algebraic form,

$$\tilde{h}(k) = \tilde{c}(k) + \tilde{c}(k)\rho\tilde{h}(k), \quad (9)$$

where $\tilde{h}(k)$ and $\tilde{c}(k)$ are the Fourier transforms of the total and direct correlation functions $h(r)$ and $c(r)$, respectively. The generalization of the OZ relation for multicomponent mixtures reads as⁴¹

$$\tilde{\mathbf{H}}(k) = \tilde{\mathbf{C}}(k) + \tilde{\mathbf{C}}(k) \cdot \mathbf{D} \cdot \tilde{\mathbf{H}}(k), \quad (10)$$

where $\tilde{\mathbf{H}}(k)$ and $\tilde{\mathbf{C}}(k)$ are $\nu \times \nu$ symmetric matrices with elements,

$$[\tilde{\mathbf{H}}(k)]_{ij} = \tilde{h}_{ij}(k) \quad \text{and} \quad [\tilde{\mathbf{C}}(k)]_{ij} = \tilde{c}_{ij}(k), \quad (11)$$

and \mathbf{D} is a $\nu \times \nu$ diagonal matrix of the partial densities,

$$[\tilde{\mathbf{D}}]_{ij} = \rho_i \delta_{ij}. \quad (12)$$

Equation (10) above generates $\nu(\nu+1)/2$ independent algebraic equations for the $\nu(\nu+1)$ unknown functions $\tilde{h}_{ij}(k)$ and $\tilde{c}_{ij}(k)$. The system becomes in principle solvable if one provides additional $\nu(\nu+1)/2$ closure equations between these functions. For example, the Rogers–Young closure generalization to multicomponent mixtures reads as

$$g_{ij}(r) = \exp[-\beta v_{ij}(r)] \left[1 + \frac{\exp[\gamma_{ij}(r)f_{ij}(r)] - 1}{f_{ij}(r)} \right] \quad (i=1,2,\dots,\nu \text{ and } i \leq j), \quad (13)$$

where $g_{ij}(r) = h_{ij}(r) + 1$, $\gamma_{ij}(r) = h_{ij}(r) - c_{ij}(r)$, and $v_{ij}(r)$ is the pair interaction between species i and j . The “mixing function” $f_{ij}(r)$ is given by

$$f_{ij}(r) = 1 - \exp(-\alpha_{ij}r). \quad (14)$$

Usually, a single self-consistency parameter $\alpha_{ij} =: \alpha$ is employed for all components, so that $f_{ij}(r) = f(r)$, as there is a single thermodynamic consistency requirement to be fulfilled, i.e., the equality of the “virial” and “fluctuation” total compressibilities of the mixture. Yet, multiparameter generalizations of the RY closure have also been proposed,⁴² invoking the partial compressibilities of the individual components. For $\alpha=0$ one recovers the Percus–Yevick (PY) and for $\alpha=\infty$ the hypernetted chain (HNC) multicomponent closures.⁴³ For a HS mixture, the PY closure is analytically solvable.^{44–46}

The RY-closure [Eqs. (10)–(14)] for the two-component mixture, using the interactions given by Eqs. (3)–(6) as inputs, was numerically solved by using the Picard-method. Monte Carlo simulations using the same interactions as inputs and measuring the structure factors at selected thermodynamics points, yielded excellent agreement with the RY closure. In our work the thermodynamic consistency of the RY closure was enforced with a single adjustable parameter α ; a simple scaling of the form $\alpha_{ij} = \alpha/\sigma_{ij}$, ($i, j = c, s$) with $\sigma_{ij} = (\sigma_i + \sigma_j)/2$ showed only small differences compared to the unscaled form.

The structure of the binary mixture is described by the three partial static structure factors $S_{ij}(k) = \delta_{ij} + \sqrt{\rho_i \rho_j} \tilde{h}_{ij}(k)$, with $i, j = c, s$. Indication of a demixing transition is the divergence of all structure factors at the long wavelength limit $k \rightarrow 0$, marking the *spinodal line* of the system. An example of a diverging structure factor is plotted in Fig. 1 together with the corresponding radial density distribution $g_{cc}(r)$. For a fixed arm number $f=32$, size ratio $q=0.5$ and colloid density $\eta_c=0.1$ we plot the colloid correlation functions for increasing star polymer packing fraction. As can be seen in Fig. 1(a), the rising contact value $g_{cc}(\sigma_c)$ signals an effective attraction between the colloids, induced by the star polymers. This is a signature of the depletion effect, to be discussed in detail below. Further increasing of

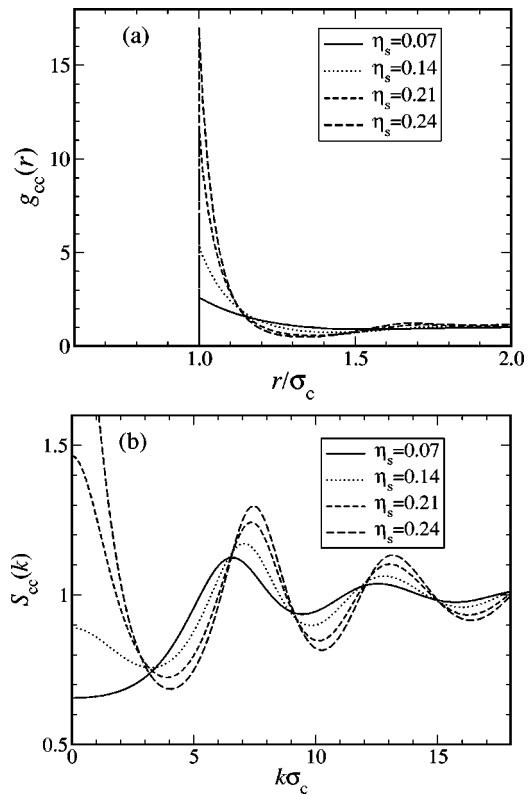


FIG. 1. (a) Radial distribution functions and (b) static structure factors for the colloids, obtained by the OZ-equations for binary mixtures closed with the RY-closure. Shown are examples for arm number $f=32$, size ratio $q=0.5$ and a fixed colloid packing fraction $\eta_c=0.1$, while the star polymer packing fraction η_s is increased. For $\eta_s=0.24$ the system is in the immediate vicinity of the spinodal line marked by the divergence of the $k \rightarrow 0$ limit of the corresponding structure factor.

the star-density, forces the system to develop long-range fluctuations and eventually to demix, as witnessed by the divergence of the low k -values in of the structure factor in Fig. 1(b).

In order to calculate the binodal lines, it is more convenient to consider the concentration structure factor, $S_{con}(k)$, which is a linear combination of the three partial structure factors. The concentration structure factor is defined as

$$S_{con}(k) = x_s^2 S_{cc}(k) + x_c^2 S_{ss}(k) - 2x_c x_s S_{cs}(k), \quad (15)$$

with the concentrations $x_i = N_i/N$, ($i = c, s$). The approach to thermodynamics is then given through the sum rule,^{7,47}

$$\lim_{k \rightarrow 0} S_{con}(k) = k_B T \left[\frac{\partial^2 g(x_s, P, T)}{\partial x_s^2} \right]^{-1}, \quad (16)$$

where $g(x_s, P, T) = G(x_s, N, P, T)/N$ is the Gibbs free energy $G(x_s, N, P, T)$ per particle and P denotes the pressure of the mixture. In order to simplify the notation, we set $x \equiv x_s$; clearly, $x_c = 1 - x$. We solved the OZ-equations for different combinations of the parameters f and q covering a wide range in the density plane (η_c, η_s) . Once the concentration structure factor, Eq. (16), is known as function of x for a fixed pressure the Gibbs free energy can be calculated by two simple integrations. In Fig. 2(a), an example for the second derivative $g''(x)$ is plotted for constant pressure \bar{P}

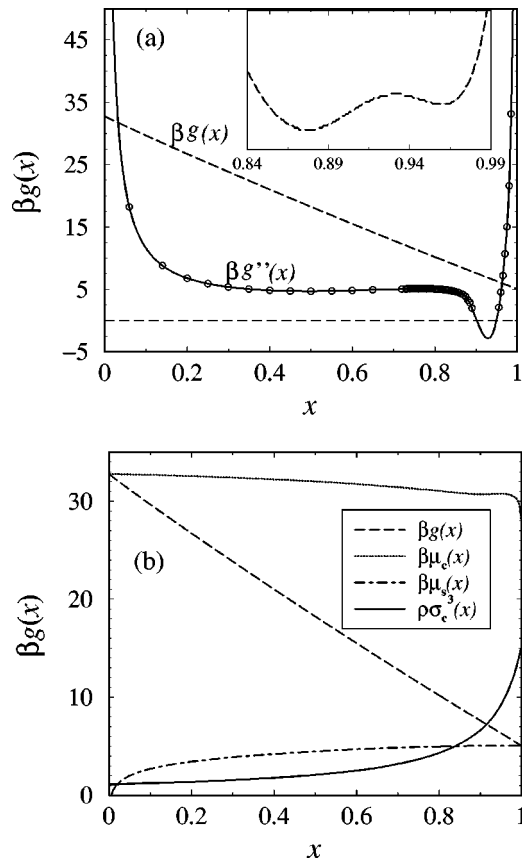


FIG. 2. (a) Example of the Gibbs free energy $g(x)$ (dashed line) plotted against the star polymer concentration $x=x_s$ in star-polymer colloid mixtures for $f=2$, size ratio $q=0.5$ and a fixed pressure $\bar{P}=28$. $g(x)$ is obtained from integration of the differential equation (16), where $S_{\text{con}}(k=0, x)$ is calculated from the OZ-equations (circles). The second derivative $g''(x)$ is interpolated by a cubic spline interpolation (solid line). The inset shows $g(x)$ after subtracting a linear function, and demonstrates the convex/concave parts of this function. (b) Partial chemical potentials of the colloids $\mu_c(x)$ and of the stars $\mu_s(x)$, plotted against the star concentration x for the same parameters as in (a). At the boundaries of $x=0$ and $x=1$, $g(x)$ (dashed line) is equal to the chemical potentials of colloids and stars, respectively. In (b), the total density $\rho\sigma_c^3(x)$ along the isobar is plotted as well.

$\equiv \beta P \sigma_c^3 = 28$, arm number $f=2$, and size ratio $q=0.5$. The Gibbs free energy is then obtained by integrating $g''(x)$ along isobars. If $g(x)$ has concave parts, [i.e., if $g''(x) < 0$ for some x -region], the system phase-separates and the boundaries are calculated by the common tangent construction on the $g(x)$ versus x curves. This common-tangent construction guarantees that partial chemical potentials of every component have the same value on both coexisting phases. As it is performed on an isobar, and for fixed temperature, the pressure and temperature are also the same between two phases and all conditions for phase coexistence are fulfilled.

The constants of integration for the calculation of $g(x)$ through the differential Eq. (16) are determined by formulating a boundary-value problem as follows. Since the Gibbs free energy is an extensive function but in its list of natural variables (N, P, x, T) only one extensive variable (N) appears, Euler's theorem asserts that the function $g = G/N$ must have the form,²

$$g(x) = (1-x)\mu_c(x) + x\mu_s(x), \quad (17)$$

where we omitted P and T from the argument list, as we are working at fixed T along an isobar. If no stars are present in the system ($x=0$) the Gibbs energy per particle reduces to the chemical potential of hard spheres at the given pressure P . To determine this, we apply the Carnahan–Starling⁴⁸ expressions for the pure hard-sphere equation of state. If no colloids are present ($x=1$), the Gibbs free energy per particle is equal to the chemical potential of the stars at the said pressure P . To determine the chemical potential of the stars for a given pressure, we calculated the equation of state of a pure star-polymer system with the one-component OZ-equation closed with RY. For $f=2$, where the star–star interaction potential is ultrasoft, it is accurate to employ a mean-field approximation^{49–53} (MFA) for the direct correlation function of the polymers, $c_{ss}(r) = -\beta V_{ss}(r)$, where $\beta = (k_B T)^{-1}$. For larger arm numbers the MFA becomes less accurate. In the MFA, use of the compressibility sum rule leads to the simple, quadratic expression for the excess Helmholtz free energy F_{ex} of the star-polymer system,⁵²

$$f_{\text{ex}} \equiv \frac{\beta F_{\text{ex}}}{V} = \frac{\rho_s^2}{2} \int \beta V_{ss}(r) d^3 r \equiv \frac{1}{2} \beta \tilde{V}_{ss}(0) \rho_s^2, \quad (18)$$

with the Fourier transform $\tilde{V}_{ss}(k)$ of the function $V_{ss}(r)$. From Eq. (18) above, we obtain the excess star chemical potential $\beta \mu_{s,\text{ex}} = \partial f_{\text{ex}} / \partial \rho_s = \beta \tilde{V}_{ss}(0) \rho_s$ and the total star chemical potential in the MFA as

$$\beta \mu_s = \ln(\rho_s \sigma_g^3) + \beta \tilde{V}_{ss}(0) \rho_s. \quad (19)$$

Through the procedure described above, the boundaries $g(x=0)$ and $g(x=1)$ are known for every pressure P and an accurate integration of $g''(x)$ can be performed. Once the exact free energy is known, all other quantities of interest can be calculated, for instance the partial chemical potentials $\mu_c(x)$ and $\mu_s(x)$ of colloids and stars, respectively, which are needed to perform the mapping of the phase diagrams from the two-component to the one-component description in Sec. III. Examples of so-determined partial chemical potentials are shown in Fig. 2(b). Some technical details on the solution of the differential Eq. (16) are presented in the Appendix.

Inside the spinodal line, the limits $S_{ij}(k \rightarrow 0)$ attain non-physical, negative values associated with the physical instability of the mixture against phase separation. Consequently, a solution of the integral equations is not possible there, and above the critical pressure P^* , the concentration structure factor $S_{\text{con}}(x, k=0)$ is unknown in some interval $\Delta x(P)$. In the example of Fig. 2(a), the interval is $0.9 < x < 0.95$. Thus, it is necessary to interpolate $S_{\text{con}}(x, k=0)$ to obtain the second derivative $g''(x)$ for all x , and this is shown as a solid line in Fig. 2(a). This way, the integration of Eq. (16) can be performed. We emphasize that the interpolation is simply done in order to facilitate the integration. The resulting binodal lines are independent of the precise interpolation scheme, as long as the integral equation theories are capable of reaching the precise spinodal, i.e., the points in which the $k \rightarrow 0$ limit of the structure factor diverges. Since this is not strictly the case, and sometimes we have to stop slightly before the spinodal is reached, there are small inaccuracies

induced by the interpolation procedure that grow with the width of the interval Δx where no solutions of the integral equation theories can be found.

In the vicinity of the critical point $\eta_c^* \approx 0.3$, the missing interval Δx is very small and the interpolation is reliable. Here the binodals should be accurate, while for higher pressures (packing fractions $\eta_c < \eta_c^*$ and $\eta_c > \eta_c^*$) the binodals are more approximate but show reasonable behavior. For highly asymmetric systems ($q \leq 0.18$) it becomes more and more difficult to get solutions of the integral equations in the vicinity of the spinodal line and the calculation of binodals is not possible.

The results for the phase boundaries in the (η_c, η_s) -plane have been presented in Ref. 26. There, semi-quantitative agreement with experimental results, without use of fit parameters in the theory, has been found. Since the chemical potential of the stars in both coexisting phases is the same, it is possible to imagine now that both are brought into partial contact with a reservoir of stars, in which the stars have this common value of the chemical potential. The word “partial” here means that the contact is assumed to materialize through a semipermeable membrane that allows the passage of star-polymers but not of colloids through it. Let η_s^r be the packing fraction of the star-polymers in the reservoir. Since the reservoir *and* the two coexisting phases all have the same value for the partial chemical potential μ_s , it follows that a representation of the phase diagram in the (η_c, η_s) -plane can be transformed, without loss of information, into the (η_c, μ_s) - or, equivalently, the (η_c, η_s^r) -plane. A comparison to the effective-one component description results where the phase diagrams are plotted in the (η_c, η_s^r) -plane will be shown in Sec. V.

III. MAPPING ONTO AN EFFECTIVE ONE-COMPONENT SYSTEM

In this section we proceed with a mapping of the two-component mixture onto an effective one-component system of colloids only, in which the star-polymers have been traced out. The result of this integration is an effective colloid–colloid interaction in which the bare, hard-sphere potential of Eq. (3) is “dressed” by a depletion interaction that has its origins in the star polymers. The star–star and star–colloid interactions enforce spatial correlations of the latter when they are brought close to two colloidal hard spheres held at separation \mathbf{R}_{12} from one another, and it is precisely these correlations that determine the form of the depletion potential. We thus present different methods in obtaining the depletion potential and compare between those. Inherent in the derivation of a depletion potential is the omission of many-body forces effectively acting between the colloids when the stars have been thermodynamically traced out.^{14,22} It will be shown that these play only a minor role, though.

A. Computer simulations

The most accurate way to calculate the effective interaction between two colloids in presence of the star polymers is to employ direct computer simulations.^{54–58} To this end, we placed two colloidal particles with coordinates \mathbf{R}_1 and \mathbf{R}_2 along the body diagonal of a cubic simulation box of volume

V , symmetrically around their center of mass that coincided with the cube center. Thus $\mathbf{R}_{12} = \mathbf{R}_2 - \mathbf{R}_1$ is the vector connecting the sphere centers and $R_{12} = |\mathbf{R}_{12}|$ is the mutual separation distance of the colloids. In addition, we introduced N_s star polymers in the same box. As there are only two colloidal spheres, we are dealing with the limit $\rho_c \rightarrow 0$, therefore the packing fraction $\eta_s = (\pi/6)(N_s/V)\sigma_g^3$ of the stars in the box can be identified with the reservoir packing fraction η_s^r introduced in the preceding section.

We performed standard *NVT*-Monte-Carlo simulations, holding the positions of the colloidal spheres fixed and taking statistics on the stars, for various different separations R_{12} between the colloids. We employed the pair potentials given by Eqs. (4) and (5) for the interaction between the stars (depending on their arm number) and by Eq. (6) for the interaction between stars and colloids. Due to the second colloid, the radial symmetry of the density distribution of the stars around one colloid is broken. A nonvanishing force is now acting on each of the colloid in direction of their connecting vector $\mathbf{R}_{12} = \mathbf{R}_2 - \mathbf{R}_1$, because of depletion or aggregation of the stars between the colloids, dependent of the distance R_{12} between them. The resulting force in directions perpendicular to their connecting vector remains zero. After a sufficiently long equilibration time, the force \mathbf{F}_1 acting on one of the colloids has been measured by performing the statistical average

$$\mathbf{F}_1(R_{12}) = \left\langle - \sum_{j=1}^{N_s} \nabla_{\mathbf{R}_1} V_{sc}(|\mathbf{R}_1 - \mathbf{r}_j|) \right\rangle_{\mathbf{R}_{12}}. \quad (20)$$

In Eq. (20) above, \mathbf{r}_j , $j = 1, 2, \dots, N_s$, stand for the positions of the star polymers, whereas the symbol $\langle \dots \rangle_{\mathbf{R}_{12}}$ denotes a constrained statistical average over the star polymers only, when the two colloids are held at separation \mathbf{R}_{12} . Due to symmetry, for the force on the second colloid it holds $\mathbf{F}_2(R_{12}) = -\mathbf{F}_1(R_{12})$ and the magnitude of the depletion force, $F_{\text{dep}}(R_{12})$, is given by

$$F_{\text{dep}}(R_{12}) = \frac{\mathbf{R}_1 - \mathbf{R}_2}{R_{12}} \cdot \mathbf{F}_1(R_{12}). \quad (21)$$

The depletion force acts for distances $R_{12} > \sigma_c$ only; for closer approaches, the bare, HS-interaction takes over. $F_{\text{dep}}(R_{12}) < 0$ denotes attractions between the colloids, mediated by the stars. Indeed, for colloid separations $R_{12} \cong \sigma_c$ such attractions are expected to show up, as in this case the two colloids are hit asymmetrically by the stars from the outside, and the unbalanced osmotic pressure of the latter pushes the hard spheres together. The total effective force acting on the first colloid in the presence of the stars is $\mathbf{F}_{\text{eff}}(R_{12}) = \mathbf{F}_{\text{HS}}(R_{12}) + \mathbf{F}_1(R_{12})$ and can be figured as the gradient of an effective potential that is a sum of the bare, hard-sphere interaction and the *depletion potential* $V_{\text{dep}}(R_{12})$,

$$\begin{aligned} \mathbf{F}_1(R_{12}) &= -\nabla_{\mathbf{R}_1} V_{\text{eff}}(R_{12}) \\ &= -\nabla_{\mathbf{R}_1} [V_{cc}(R_{12}) + V_{\text{dep}}(R_{12})]. \end{aligned} \quad (22)$$

In Fig. 3, we show representative examples for the resulting depletion force $F_{\text{dep}}(R_{12})$ for various different functionalities and size ratios. The figure shows also a compari-

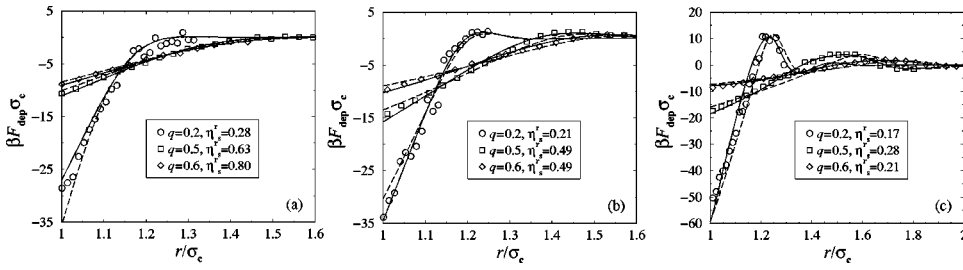


FIG. 3. Depletion forces for different functionalities f and size ratios q . (a) $f=2$; (b) $f=6$; (c) $f=32$. The symbols denote simulation results, the solid lines the force resulting from the inversion of the RY-closure and the broken lines the results of the superposition approximation. The denoted values of the reservoir star-polymer packing fractions, η_s^r , were chosen to be close to the demixing critical point in the fluid phase.

son with results of the inversion of OZ-equations, see Sec. III B and of the superposition approximation, Sec. III C. The disadvantage of the use of simulations for calculating depletion forces is the need of many long runs for high resolved curves with good statistics. Referring to this figure, we note that for $f=2$ we recover essentially the Asakura–Oosawa-result,¹⁴ with the depletion force being purely attractive, Fig. 3(a). Increasing the star functionality, however, leads to an oscillatory behavior of the effective force, which is caused by the increasingly strong correlation effects between the stars, see Figs. 3(b) and 3(c). This characteristic is akin to the features of the depletion force found in binary hard-sphere mixtures.^{24,59} Star polymers act as depleting agents that interpolate between the linear polymer behavior and the hard-sphere one.

B. Inversion of the OZ equation for binary mixtures

An alternative route to the depletion potential, which does not require the use of computer simulations, is offered by the so-called inversion of the full, two-component integral-equation theory—results in the limit of low colloid density.^{25,60,61} Indeed, it follows from exact diagrammatic expansions in the theory of liquids⁴³ that the radial distribution function $g(r)$ attains in the low-density limit the form $g(r) = \exp[-\beta v(r)]$, with $v(r)$ denoting the pair potential acting between the constituent species of the fluid. Thereby, the effective potential $V_{\text{eff}}(r)$ acting between the colloids and depending parametrically on the star-reservoir packing fraction η_s^r can be obtained by solving the two-component Ornstein–Zernike equations with the Rogers–Young closure for given star packing fraction η_s^r and at the limit $\eta_c \rightarrow 0$. The so-obtained colloid–colloid radial distribution function $g_{cc}(r)$ can be then inverted employing the exact relation above and yielding the effective potential as

$$\beta V_{\text{eff}}(r) = - \lim_{\eta_c \rightarrow 0} \ln [g_{cc}(r; \eta_c, \eta_s^r)]. \quad (23)$$

In Fig. 3 we show results for the effective force $F_{\text{eff}}(r) = -\nabla V_{\text{eff}}(r)$ derived from $\beta V_{\text{eff}}(r)$ obtained by the procedure outlined above, in comparison with the simulation results of Sec. III A. Excellent agreement between the two is found, for all (q, f) parameter combinations considered. Small deviations for distances near contact $r \approx \sigma_c$ could be corrected by introducing a simple scaling for the consistency parameter $\alpha_{ij} = \alpha/\sigma_{ij}$, ($i, j = c, s$) with an auxiliary ratio parameter $q' = \sigma_s/\sigma_c = 0.5$ used for all size ratios q and all arm numbers f .

C. Superposition approximation

A third way to the depletion potential is offered by the so-called *superposition approximation* (SA) of Attard.⁶² If the exact star-polymer density distribution $\rho_s(\mathbf{r}_1; \mathbf{R}_1, \mathbf{R}_2)$ at \mathbf{r}_1 around two colloids held fixed at positions \mathbf{R}_1 and \mathbf{R}_2 were known, then the depletion force in the low-density limit could be calculated by an integration over the contributions of the force between star-polymers and a colloid in direction of $\mathbf{R}_{12} = \mathbf{R}_2 - \mathbf{R}_1$. As a matter of fact, the density $\rho_s(\mathbf{r}_1; \mathbf{R}_1, \mathbf{R}_2)$ is proportional to the three-body, star-colloid–colloid distribution function $g_{scc}^{(3)}(\mathbf{r}_1, \mathbf{R}_1, \mathbf{R}_2)$. Since the latter is in general unknown, in the SA it is factorized as a product of pair distribution functions, as explained below.

Let us consider two colloids in a distance R_{12} , as depicted in Fig. 4. We put the origin of our coordinate system in the center of one of the two colloids surrounded by star-polymers with density $\rho_s(\mathbf{r}_1; \mathbf{R}_1, \mathbf{R}_2)$. The depletion force acting on the left sphere is given by the general relation, Eq. (20). Taking into account that $\nabla_{\mathbf{R}_1} V_{sc}(|\mathbf{R}_1 - \mathbf{r}_1|) = -\nabla_{\mathbf{r}_1} V_{sc}(|\mathbf{R}_1 - \mathbf{r}_1|)$, setting $\mathbf{R}_1 = 0$, performing the statistical average there, and projecting on the \mathbf{R}_{12} direction according to Eq. (21), we obtain the depletion force as

$$F_{\text{dep}}(R_{12}) = -2\pi \int_0^\infty r_1^2 \frac{dV_{sc}(r_1)}{dr_1} dr_1 \times \int_{-1}^1 \rho_s(\mathbf{r}_1; \mathbf{R}_1, \mathbf{R}_2) \omega d\omega, \quad (24)$$

where $\omega = \cos \theta$.

The superposition approximation amounts to replacing the exact density $\rho_s(\mathbf{r}_1; \mathbf{R}_1, \mathbf{R}_2)$ of the stars in the presence of the two colloids by the product of the bulk star density ρ_s^r

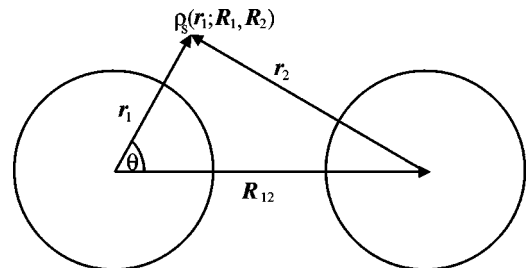


FIG. 4. A sketch of two colloids in a distance R_{12} . The origin of the coordinates lies in the center of the left sphere. $\rho_s(\mathbf{r}_1; \mathbf{R}_1, \mathbf{R}_2)$ is the star-polymer density at \mathbf{r}_1 , in the presence of the two colloids at positions \mathbf{R}_1 and \mathbf{R}_2 .

times the two radial distribution functions on the stars in the presence of two *isolated* colloids, one with its center at \mathbf{R}_1 and one with its center at \mathbf{R}_2 . Hence, in the SA one writes

$$\rho_s(\mathbf{r}_1; \mathbf{R}_1, \mathbf{R}_2) \approx \rho_s^r g_{cs}(|\mathbf{r}_1 - \mathbf{R}_1|) g_{cs}(|\mathbf{r}_1 - \mathbf{R}_2|), \quad (25)$$

where, evidently, $\rho_s^r = (6\eta_s^r)/(\pi\sigma_s^3)$ relates the reservoir density and packing fraction. The radial distribution functions $g_{cs}(|\mathbf{r}_1 - \mathbf{R}_i|)$ above relate to a sea of stars in the presence of a single colloid, hence they are readily available by the $\eta_c \rightarrow 0$ -limit of the two-component integral equation theories. Noting that $|\mathbf{r}_1 - \mathbf{R}_2| = |\mathbf{r}_2| = \sqrt{R_{12}^2 + r_1^2 - R_{12}r_1\omega}$, we finally obtain in the SA,

$$F_{\text{dep}}(R_{12}) = -2\pi\rho_s^r \int_0^\infty r_1^2 \frac{dV_{sc}(r_1)}{dr_1} g_{cs}(r_1) dr_1 \times \int_{-1}^1 g_{cs}(\sqrt{R_{12}^2 + r_1^2 - R_{12}r_1\omega}) \omega d\omega. \quad (26)$$

In Fig. 3 we show results obtained from this approximation, in comparison to direct simulation results and to the inversion presented in the preceding subsection. It can be seen that superposition approximation reproduces the simulation results in the linear polymer limit, $f=2$, very well. In this case, the star polymer are very soft, weakly interacting particles. Thereby, the cross-correlations between them arising from the interaction $V_{ss}(r)$ are so weak that the superposition approximation is valid: the presence of a second colloid results into a density profile for the stars that is very well approximated by the product of those arising from two isolated colloids. However, for larger functionalities, where the star–star interaction starts causing significant correlation effects between them, the resulting depletion interactions and forces from the SA are less accurate. As expected, the SA underestimates the degree of oscillatory behavior of the force; in addition, the phase of those oscillations is in error. Thus, for large arm numbers, the superposition approximation is not an adequate tool for calculating accurately the effective interaction.

IV. PHASE DIAGRAMS

Due to the shortcomings of the superposition approximation and the accuracy of the inversion of the RY-results, we have resorted to the latter procedure in order to calculate the depletion potential. Some examples of this potential are plotted in Fig. 5 for different arm numbers f and reservoir packing fractions η_s^r of the stars. Employing this interaction, we proceed with the calculation of the phase diagrams of selected star-polymer–colloid mixtures. The goal is to establish the limits of stability of the demixing transition with respect to the crystallization of the colloids. Thereby, we limited ourselves to the common, fcc-structure for candidate colloidal crystals, which materializes for colloids in the absence of stars ($\eta_s^r=0$). Though competing crystal structures cannot be ruled out a priori, the quantitative features of the depletion potential render the stability of more open crystal structures, such as the bcc-lattice, improbable. For the calculation of the phase diagrams, we combined simulations and perturbation theory, as explained below.

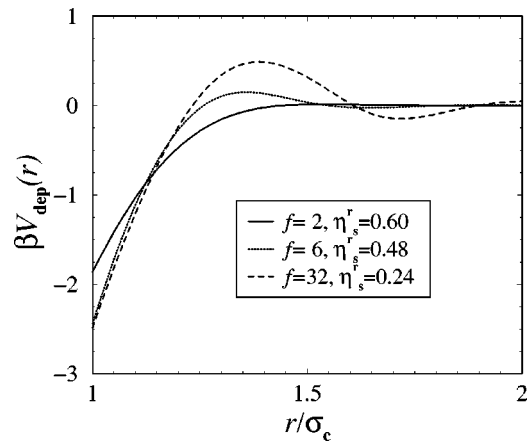


FIG. 5. Depletion potentials $V_{\text{dep}}(r)$ for the colloids obtained by mapping the two-component system on an effective one-component system by inversion of OZ-equations in the low-density limit. We plot the potential for different arm numbers $f=2,6,32$ for star polymer reservoir packing fractions η_s^r near the critical point of fluid demixing. The size ratio is $q=0.5$.

A. Simulation

In order to determine phase coexistence, it is necessary to calculate the Helmholtz free energy $F = F(N_c, V, \eta_s^r)$. An accurate but computational expensive way is to perform thermodynamical integration of Monte Carlo simulation results, using the hard-sphere system as reference; for a detailed description, see Refs. 14 and 59. The free energy can be integrated as

$$F(N_c, V, \eta_s^r) = F_0(N_c, V, \eta_s^r=0) + \int_0^1 d\lambda \left\langle \sum_{i<j}^{N_s} V_{\text{dep}}(r) \right\rangle_{N_c, V, \eta_s^r, \lambda}, \quad (27)$$

while using an auxiliary effective interaction $V_{\text{eff}}^\lambda(r)$ between the star-polymers and colloids in the simulation,

$$V_{\text{eff}}^\lambda(r) = V_{cc}(r) + \lambda V_{\text{dep}}(r). \quad (28)$$

Here, $0 \leq \lambda \leq 1$ is a dimensionless coupling parameter, interpolating between the hard sphere reference interaction ($\lambda = 0$) and the effective potential $V_{\text{eff}}(r)$. For the free energy of the hard sphere reference system, $F_0(N_c, V, \eta_s^r=0)$, we use the Carnahan–Starling expression⁴⁸ for the fluid, and the equation of state proposed by Hall⁶³ for the solid phase. The calculation for every point on the free energy curve was performed with $N_s = 108$ particles starting with a face-centered-cubic configuration. After fitting polynomials to the function $f(\rho_c) = F/V$, a common tangent construction was employed to obtain the coexistence curves among all phases.

B. Perturbation theory

A theoretical understanding of the effects of the depletion potential can be reached within the framework of standard perturbation theory, using the hard-sphere system as reference. To first order in perturbation theory, the Helmholtz free energy of a collection of colloids interacting by the hard-sphere plus depletion potentials is given by⁴³

$$\frac{\beta F}{N_c} = \frac{\beta F_0}{N_c} + \frac{1}{2} \beta \rho_c \int g_0(r) \phi(r) d^3 r, \quad (29)$$

where F_0 and $g_0(r)$ are the free energy and radial pair correlation function of the reference system, and $\phi(r)$ the perturbing potential, $V_{\text{dep}}(r)$ in this case. Barker and Henderson developed a second order term, including two-body correlations,⁶⁴ and refining thereby the perturbation theory for the free energy into

$$\begin{aligned} \frac{\beta F}{N_c} = & \frac{\beta F_0}{N_c} + \frac{1}{2} \beta \rho_c \int g_0(r) \phi(r) d^3 r \\ & - \frac{1}{4} \left(\frac{\partial \rho}{\partial p} \right)_0 \beta \rho_c \int g_0(r) \phi^2(r) d^3 r. \end{aligned} \quad (30)$$

In Eq. (30) above, $(\partial \rho / \partial p)_0$ is the compressibility of the reference system. For the reference free energy F_0 , we used the expressions of Canahan–Starling and Hall, for the fluid and solid phase, respectively. The pair distribution functions $g_0(r)$ are provided by the parametrizations of Verlet and Weis⁶⁵ for the fluid phase and Kincaid and Weis⁶⁶ for the solid. Free energy calculations using Eq. (30) were performed by Dijkstra *et al.* for the effective Asakura–Oosawa pair potential, modeling colloid–polymer mixtures¹⁴ and for the effective one-component system arising by integrating out the small spheres in a binary hard sphere mixture.⁵⁹ It was found there that this approach yields excellent agreement for the fluid–solid boundaries compared to thermodynamical integration results.

C. Results

As far as the star-polymer–colloid mixtures are concerned, we find from the comparison of the Helmholtz free energy calculated from the two different approaches described above, that the two are in excellent agreement as far as the solid branch of the free energy is concerned. This is consistent with the findings in Refs. 14 and 59. For the fluid branch, though, only the low density range coincide, for larger densities the free energy of the perturbation approach is always too large. This result is consistent with the fact that the first-order perturbation theory arises from the Gibbs–Bogolyubov inequality and hence the resulting free energy can only be larger than the true one. Moreover, in the fluid phase, the hard-sphere radial distribution function $g_0(r)$ severely underestimates the contact value of the true $g(r)$, thus resulting in an internal energy that is significantly higher than the true one at intermediate and high fluid densities. Thus, the Helmholtz free energy of the fluid is overestimated. In view of the inaccuracy of the perturbation theory for the fluid phase, we resorted to the results of the Monte Carlo simulation, whereas for the solid we employed the perturbation approach, in order to reduce the computational effort.

In Fig. 6 we plot the phase diagrams for arm numbers $f=2, 6,$ and 32 and size ratios $q=0.2, 0.5,$ and 0.6 . For $f=2$ we obtain phase diagrams that are very similar to the ones obtained for the AO-model.¹⁴ This is interesting since in this work we are dealing with realistic polymer–polymer as well as polymer–colloid interactions, that go beyond the

simple approximations of the AO-model. Apparently, the overall features of such mixtures and, in particular, the (meta)stability of the demixing transition are insensitive to the details of the interaction potentials. At size ratio $q=0.5$, we have a demixing binodal that is only slightly stable, a result in agreement with that of Ref. 14 in which it was found $q_c \cong 0.45$.

An increase of the functionality f suppresses the stability of the demixing binodals, a finding which is in line with the general trend that, as f grows, star-polymers become more akin to hard spheres; in a mixture of hard spheres, no demixing takes place.^{17,18,59} For $f=6$, a stable demixing binodal appears at larger size ratio, $q=0.6$, see Fig. 6(b). This is to be expected, as for larger f the star-polymers become more akin to hard depletants and hence a depletion force of longer range is necessary in order to bring about phase separation in the fluid phase. For the case $f=32$ we obtain demixing binodals that are always metastable with respect to freezing, in the domain $q \leq 0.7$ in which the pair potentials are reliable. The results show a clear trend from the AO-type behavior, valid for $f=2$, to the BHS-behavior, valid for $f=32$. In view of the fact that the critical value q_c for $f=6$ seems to lie slightly below 0.6 and is growing with f , we anticipate that star polymers with $f \geq 10$ will not be able to bring about stable demixing transitions in a star-polymer–colloid mixture. For $q=0.2$, shown in Figs. 6(g), 6(h), and 6(i), we obtain no stable demixing transitions for any of the three functionalities $f=2, 6,$ and 32 that we checked. At small size ratios, star-polymers are weak depletants, causing an attraction whose range is too short to bring about a thermodynamically stable “liquid-gas” coexistence curve. Our findings are consistent with earlier results on, e.g., the hard-sphere-attractive-Yukawa system^{67,68} and other model potentials,⁶⁹ in which it was found that the liquid disappears when the range of the attractions becomes, roughly, less than 20% of that of the repulsions.

The mapping onto the one-component, depletionlike picture greatly facilitates the calculation of the phase diagrams, in particular in the crystalline state. Nevertheless, performing this mapping remains a matter of convenience; the physics should not depend on the point of view and, in particular, in an exact mapping both the phase boundaries and the correlation functions of the colloids should be identical in both pictures.²² Since we have employed approximations at various stages, in both the two-component and in the depletion approaches, it is useful to perform a comparison between the two in order to judge their severity. This is the subject of the following section.

V. COMPARISON BETWEEN THE TWO- AND ONE-COMPONENT DESCRIPTIONS

A. Phase behavior

The determination of the partial chemical potentials in the full two-component system described in Sec. II enables us to compare the results obtained there in the (η_c, η_s) - or *system*-representation, with the results obtained in Sec. IV in the (η_c, η_s^r) - or *reservoir*-representation. As we can see from Eq. (17), the partial chemical potentials of the stars and col-

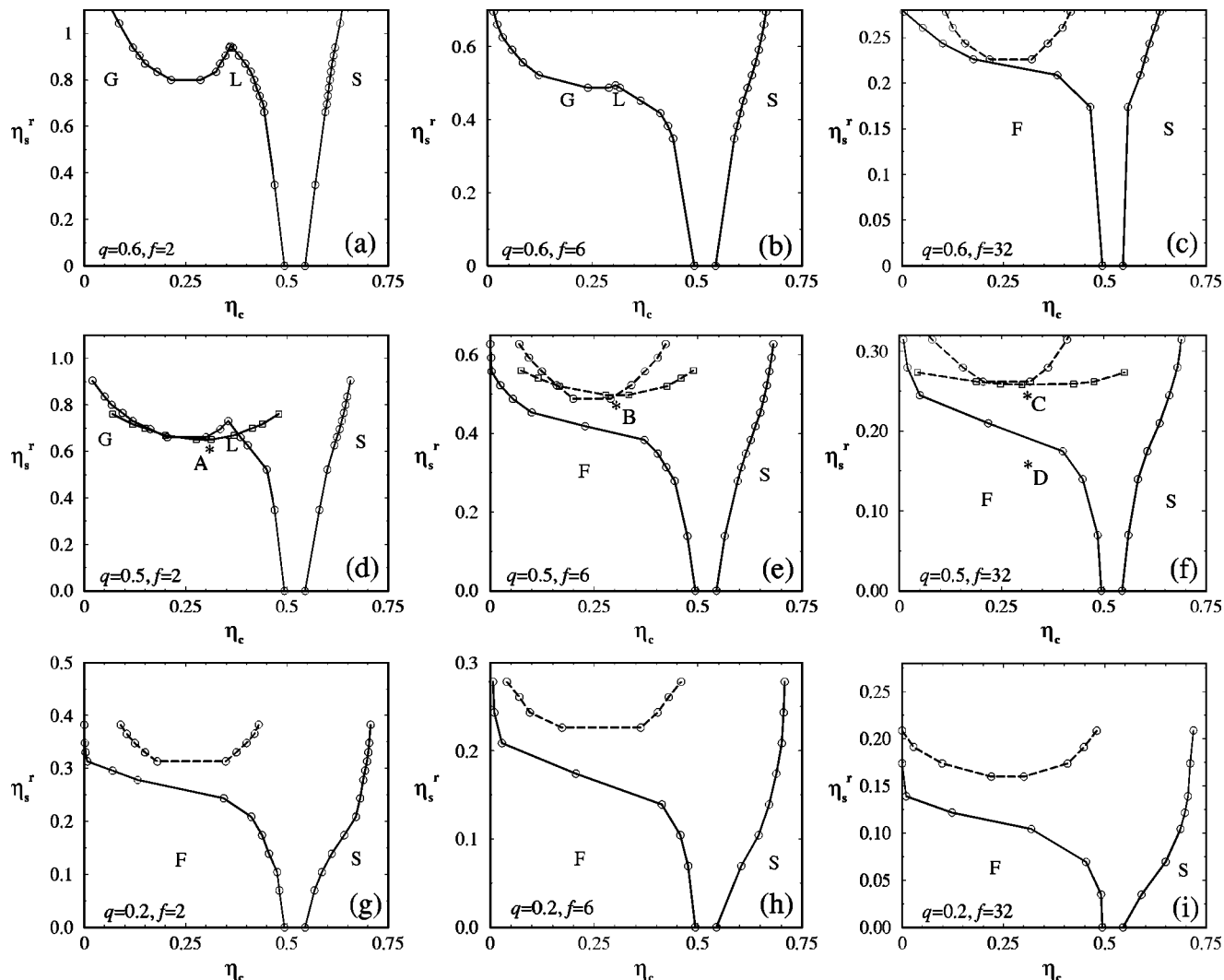


FIG. 6. Phase diagrams of star-polymer–colloid mixtures for different size ratios and different star functionalities. The circles indicate the calculated phase boundaries from the one-component description, the squares from the full two-component description, see Sec. II. The lines are a guide to the eye. The solid lines denote stable phase transitions and the broken ones metastable demixing binodals. The first row shows the phase behavior for a size ratio $q=0.6$. (a) $f=2$; (b) $f=6$; (c) $f=32$. For $f=2$ and $f=6$ the demixing transition in the fluid phase is stable, resulting into three distinct phases: gas (G), liquid (L), and solid (S). For $f=32$ the freezing transition preempts demixing, resulting into two stable phases: fluid (F) and solid (S). In the second row the phase behavior for $q=0.5$ is plotted, again the arm number increases from (d) to (f), in analogy to the first row. Now only for $f=2$ a stable demixing binodal is found. The asterisks denote state points at which pairwise correlation functions were calculated. The last row shows the behavior for $q=0.2$. No stable fluid–fluid transition is observed for arm numbers $f=2$ (g), $f=6$ (h), and $f=32$ (i).

loids can be simply obtained by the common tangent construction; the intersection of the tangent with the $x=0$ or $x=1$ axis yield the partial chemical potential μ_c or μ_s , respectively. Now, for every two coexistence points in the (η_c, η_s) ensemble we determine the corresponding chemical potential μ_s . The equation of state of the one component star polymer system determined by RY gives us the reservoir packing fraction to every chemical potential. We calculate the transformed curves for a size ratio $q=0.5$ and arm numbers $f=2, 6, \text{ and } 32$. The results of the mapping of the coexistence points from the (η_c, η_s) -plane into the (η_c, η_s^r) -plane are shown in Figs. 6(d)–6(f) together with the fluid-demixing binodals from the one-component approach. Regarding the critical points the agreement is very good. Although many-body terms are neglected in the effective one-component description,^{14,22} we find a satisfactory agreement, both for the critical colloid density and for the critical

star polymer reservoir density. Away from the critical point, the coexistence lines from the two-component approach are too broad. The farther one is from the critical point, the more difficult it becomes to reach precisely the spinodal of the mixture and then the numerical inaccuracies caused by the interpolation in the neighborhood of the spinodal become more and more relevant.

B. Structure

We now discuss the colloid–colloid correlation functions in the fluid phase. We showed how to translate the star polymer densities on the phase boundaries to the corresponding chemical potentials or reservoir packing fractions. Hence, we are able to compare the structure of the colloids in the one- and two-component description on selected state points of the phase diagrams. In Fig. 7 we plot the pair distribution

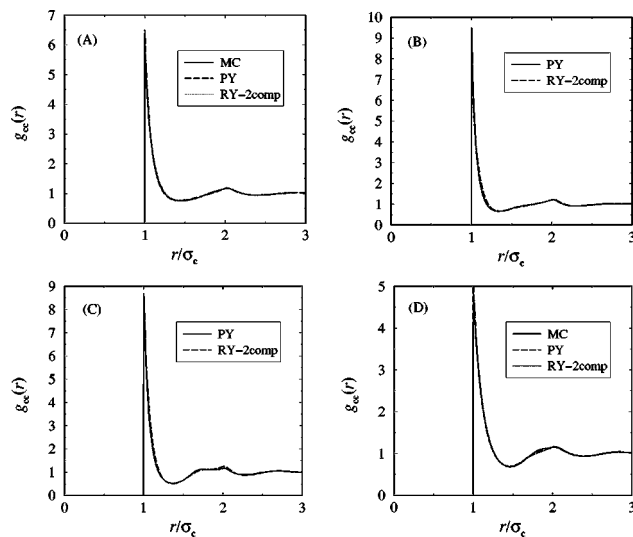


FIG. 7. Comparison of the pair correlations functions $g_{cc}(r)$ for the colloids at different state points (A)–(D), denoted by the asterisks in the phase diagram for $q=0.5$ in (d)–(f). Using the depletion potentials from the one-component description MC simulations (solid lines) are compared to PY results (dashed lines). Dotted lines present RY-results employing the full binary OZ-equations.

function $g_{cc}(r)$ and in Fig. 8 the associated static structure factors $S_{cc}(k)$ corresponding to four different state points (A)–(D) in the phase diagram Fig. 6. The size ratio is $q = 0.5$ and the arm numbers f vary. The state points (A)–(C) are chosen to be close to the fluid-fluid demixing critical point, while point (D) is deep in the stable fluid phase. For the one-component system we use the Percus–Yevick (PY)-closure, which is expected to be accurate for the short-ranged interactions between the colloids. For the two-component case, we use the RY-closure as described in Sec. II. In addition we compute the correlation functions with computer

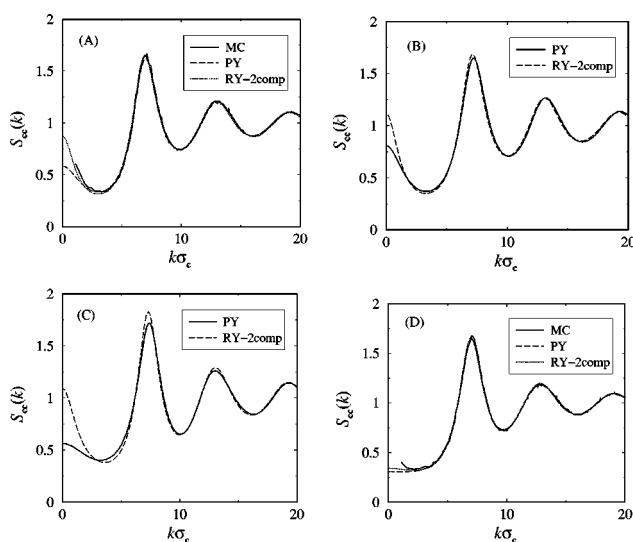


FIG. 8. Comparison of the static structure factors $S_{cc}(q)$ for the colloids at different state points (A)–(D), denoted by the asterisks in the phase diagram for $q=0.5$ in (d)–(f). Using the depletion potentials from the one-component description MC simulations (solid lines) are compared to PY results (dashed lines). Dotted lines present RY-results employing the full binary OZ-equations.

simulations for the state points (A) and (D), where the fluid demixing transition is not preempted by freezing. In the simulations the structure factor was calculated directly, using⁴³

$$S_{cc}(k) = N_c^{-1} \langle \rho_c(\mathbf{k}) \rho_c(-\mathbf{k}) \rangle, \quad (31)$$

where $\rho_c(\mathbf{k})$ is the Fourier transform of the colloid one-particle density operator and is defined as⁴³

$$\rho_c(\mathbf{k}) = \sum_{i=1}^{N_c} \exp(i\mathbf{k} \cdot \mathbf{r}_i), \quad (32)$$

with the sum being extended over all positions \mathbf{r}_i of the N_c colloidal particles.

The simulations were performed using the same one-component effective interactions as the PY-calculations. First of all, the agreement between PY and simulations data demonstrates that the PY-closure yields very good results for the structure in systems with a hard-sphere interaction dressed with a short-range attraction, as also seen in Refs. 14 and 70. Further, the $S_{cc}(k)$'s resulting from the solution of the two-component system (through the RY-closure) are indeed very similar to those arising from the solution of the effective one-component system (through the PY-closure) at the corresponding thermodynamic points. This demonstrates the validity of the mapping procedure and also serves as an indirect proof that higher-order interactions, which have been neglected in the one-component description, are not crucial.^{71,72} The structure factors at the thermodynamic points (A), (B), and (C) show the typical enhancement for low k -values, due to their close distance from the demixing spinodal. The faster divergence of the RY-structure factor in comparison with the PY- one is in line with the demixing spinodals and demonstrates the superiority of the RY-closure with respect to PY regarding thermodynamic properties.

VI. SUMMARY AND CONCLUDING REMARKS

We have traced out the phase diagram of star-polymer–colloid mixtures, establishing the limits of stability of the demixing binodals as functions of the star functionality and the size ratio, for the case in which the star-polymers are smaller than the colloids. We have demonstrated the equivalence of a two-component approach with a depletion picture, in which the stars are further traced out. Star polymers have been shown to fulfill their unique role as natural bridging systems between soft polymers (for low f) and colloidal particles (at high f). Hence, they can act as selective depletants between colloidal hard spheres. All our findings can be experimentally checked by carefully preparing mixtures of index-matched hard sphere colloids with monodisperse star-polymers in good solvents.²⁶

The stability of the demixing with respect to freezing has been recently studied in some generality in the framework of the model of nonadditive hard spheres.^{18,73,74} Whether the present system can also fit within this picture remains to be seen. Our work is limited to star-colloid size ratios smaller than unity, since the star-colloid interactions employed here are derived under the assumption that the star never “crawls over” the colloidal hard sphere.³⁵ The investigation of the

opposite case, in which the small colloids can fully penetrate into the corona of the star-polymers⁷⁵ is also a problem for the future.

ACKNOWLEDGMENTS

The authors thank A. A. Louis for helpful discussions. This work has been supported by the Deutsche Forschungsgemeinschaft through the SFB 237.

APPENDIX: ON THE $x \rightarrow 0$ AND $x \rightarrow 1$ LIMITS OF THE GIBBS FREE ENERGY

In this Appendix we present some technical details necessary for the solution of the second-order differential Eq. (16). With the Gibbs free energy per particle,

$$g(x) = \frac{G(x, T, P)}{N}, \tag{A1}$$

we seek to solve the equation,⁴⁷

$$g''(x) = \frac{k_B T}{S_{\text{con}}(k=0)}, \tag{A2}$$

where it is implied that the pressure P and the temperature T are constant.

The concentration structure factor $S_{\text{con}}(k)$ for a colloid-star mixture of partial concentrations x_c and x_s is defined as

$$\begin{aligned} S_{\text{con}}(k) &= \frac{1}{N} \langle [x_s \rho_c(\mathbf{k}) - x_c \rho_s(\mathbf{k})] \\ &\quad \times [x_s \rho_c(-\mathbf{k}) - x_c \rho_s(-\mathbf{k})] \rangle \\ &= x_s^2 \frac{1}{N} \langle \rho_c(\mathbf{k}) \rho_c(-\mathbf{k}) \rangle + x_c^2 \frac{1}{N} \langle \rho_s(\mathbf{k}) \rho_s(-\mathbf{k}) \rangle \\ &\quad - 2x_c x_s \frac{1}{N} \langle \rho_c(\mathbf{k}) \rho_s(-\mathbf{k}) \rangle, \end{aligned} \tag{A3}$$

where $\rho_c(\mathbf{k})$ is defined through Eq. (32) and similarly for $\rho_s(\mathbf{k})$.

We define the partial structure factors $S_{ij}(k)$ as $S_{ij}(k) = \delta_{ij} + \sqrt{\rho_i \rho_j} \tilde{h}_{ij}(k)$, $i, j = c, s$. It can be shown⁴³ that these $S_{ij}(k)$'s satisfy the equations,

$$x_c S_{cc}(k) = \frac{1}{N} \langle \rho_c(\mathbf{k}) \rho_c(-\mathbf{k}) \rangle, \tag{A4}$$

$$x_s S_{ss}(k) = \frac{1}{N} \langle \rho_s(\mathbf{k}) \rho_s(-\mathbf{k}) \rangle, \tag{A5}$$

$$\sqrt{x_c x_s} S_{cs}(k) = \frac{1}{N} \langle \rho_c(\mathbf{k}) \rho_s(-\mathbf{k}) \rangle. \tag{A6}$$

From Eqs. (A3) to (A6) we obtain

$$\begin{aligned} S_{\text{con}}(k) &= x_c x_s^2 S_{cc}(k) + x_s x_c^2 S_{ss}(k) \\ &\quad - 2(x_c x_s)^{3/2} S_{cs}(k). \end{aligned} \tag{A7}$$

We now set $x_s = x$, $x_c = 1 - x$ and introduce the total density ρ of the mixture, related to the partial densities through $\rho_c = (1 - x)\rho$ and $\rho_s = x\rho$. Using $S_{ij}(k) = \delta_{ij} + \sqrt{\rho_i \rho_j} \tilde{h}_{ij}(k)$ and Eqs. (A2) and (A7) above, we obtain

$$\begin{aligned} \beta g''(x) &= \{x^2(1-x)[1 + (1-x)\rho \tilde{h}_{cc}(0)] \\ &\quad + x(1-x)^2[1 + x\rho \tilde{h}_{ss}(0)] \\ &\quad - 2x^2(1-x)^2\rho \tilde{h}_{cs}(0)\}^{-1}. \end{aligned} \tag{A8}$$

The quantities $\tilde{h}_{ij}(0)$ are all finite and so is ρ . An analysis of the limiting behavior of the rhs of Eq. (A8) above, shows that it diverges as $1/x$ for $x \rightarrow 0$ and as $1/(1-x)$ for $x \rightarrow 1$. In order to circumvent this technical difficulty at the two boundaries of integration and deal always with finite values, we split the Gibbs free energy per particle $g(x)$ into the ideal part, $g_{\text{id}}(x)$, and the excess part, $g_{\text{ex}}(x)$, as follows:

$$\begin{aligned} \beta g(x) &= \beta g_{\text{id}}(x) + \beta g_{\text{ex}}(x) \\ &= (1-x)\beta\mu_{c,\text{id}}(x) + x\beta\mu_{s,\text{id}}(x) + \beta g_{\text{ex}}(x) \\ &= (1-x)\ln[(1-x)\rho\sigma_c^3] + x\ln(x\rho\sigma_c^3) \\ &\quad + \beta g_{\text{ex}}(x) + 3(1-x)\ln\left(\frac{\Lambda_c}{\sigma_c}\right) + 3x\ln\left(\frac{\Lambda_s}{\sigma_c}\right) \\ &= (1-x)\ln(1-x) + x\ln x + \beta g_{\text{ex}}(x) + C_1 x + C_0, \end{aligned} \tag{A9}$$

where $\Lambda_{c,s}$ are the thermal de Broglie wavelengths of the colloids and stars, respectively, and in the last line we have simply introduced two constants, C_0 and C_1 for a term in $g(x)$ that is linear in x and plays no role, neither in the argument that follows nor in the determination of phase boundaries. Taking the second derivative in Eq. (A9) above, we obtain

$$\beta g''(x) = \frac{1}{x} + \frac{1}{1-x} + g''_{\text{ex}}(x). \tag{A10}$$

Thus, the $1/x$ -divergence at $x \rightarrow 0$ and the $1/(1-x)$ -divergence at $x \rightarrow 1$ manifest also in Eq. (A8) above, are seen to arise from the ideal part of the Gibbs free energy. Hence, a second-order differential equation for which all terms that appear are free of divergences can be written, which reads as

$$\beta g''_{\text{ex}}(x) = \frac{1}{S_{\text{con}}(k=0)} - \left(\frac{1}{x} + \frac{1}{1-x}\right). \tag{A11}$$

We solved therefore numerically Eq. (A11) for the determination of the function $g_{\text{ex}}(x)$; addition of the analytically known term $g_{\text{id}}(x)$ delivers the total Gibbs free energy per particle.

¹We ignore here the possibility of formation of a quasicrystal because, in practice, quasicrystal forming materials are usually ternary mixtures.

²L. D. Landau and E. M. Lifshitz, *Course of Theoretical Physics: Statistical Physics*, 3rd ed. (Pergamon, Oxford, 1980), Vol. 5.

³P. N. Pusey, in *Liquids, Freezing, and the Glass Transition*, edited by J. P. Hansen, D. Levesque, and J. Zinn-Justin (North-Holland, Amsterdam, 1991).

⁴M. Dijkstra, *Curr. Opin. Colloid Interface Sci.* **6**, 372 (2001).

⁵E. J. Meijer and D. Frenkel, *Physica A* **213**, 130 (1995).

⁶R. P. Sear and D. Frenkel, *Phys. Rev. E* **55**, 1677 (1997).

⁷T. Biben and J.-P. Hansen, *Phys. Rev. Lett.* **66**, 2215 (1991).

⁸T. Biben, P. Bladon, and D. Frenkel, *J. Phys.: Condens. Matter* **8**, 10799 (1996).

⁹D. Frenkel, *Physica A* **263**, 26 (1999).

- ¹⁰S. Asakura and F. Oosawa, *J. Polym. Sci.* **33**, 183 (1958).
- ¹¹A. Vrij, *Pure Appl. Chem.* **48**, 471 (1976).
- ¹²A. P. Gast, C. K. Hall, and W. B. Russel, *J. Colloid Interface Sci.* **96**, 251 (1983).
- ¹³H. N. W. Lekkerkerker, W. C. K. Poon, P. N. Pusey, A. Stroobants, and P. B. Warren, *Europhys. Lett.* **20**, 559 (1992).
- ¹⁴M. Dijkstra, J. M. Brader, and R. Evans, *J. Phys.: Condens. Matter* **11**, 10079 (1999).
- ¹⁵M. Schmidt, H. Löwen, J. M. Brader, and R. Evans, *Phys. Rev. Lett.* **85**, 1934 (2000).
- ¹⁶S. M. Ilett, A. Orrock, W. C. K. Poon, and P. N. Pusey, *Phys. Rev. E* **51**, 1344 (1995).
- ¹⁷M. Dijkstra, R. van Roij, and R. Evans, *Phys. Rev. Lett.* **81**, 2268 (1998).
- ¹⁸R. Roth, R. Evans, and A. A. Louis, *Phys. Rev. E* **64**, 051202 (2001).
- ¹⁹S. W. Rick and A. D. J. Haymet, *J. Chem. Phys.* **90**, 1188 (1989).
- ²⁰A. R. Denton and N. W. Ashcroft, *Phys. Rev. A* **42**, 7312 (1990).
- ²¹X. C. Zeng and D. Oxtoby, *J. Chem. Phys.* **93**, 4357 (1990).
- ²²C. N. Likos, *Phys. Rep.* **348**, 267 (2001).
- ²³B. Götzelmann, R. Roth, S. Dietrich, M. Dijkstra, and R. Evans, *Europhys. Lett.* **47**, 398 (1999).
- ²⁴R. Roth, R. Evans, and S. Dietrich, *Phys. Rev. E* **62**, 5360 (2000).
- ²⁵J. Dzubiella, C. N. Likos, and H. Löwen, *Europhys. Lett.* **58**, 133 (2002).
- ²⁶J. Dzubiella, A. Jusufi, C. N. Likos *et al.*, *Phys. Rev. E* **64**, 010401(R) (2001).
- ²⁷T. A. Witten and P. A. Pincus, *Macromolecules* **19**, 2509 (1986).
- ²⁸C. N. Likos, H. Löwen, M. Watzlawek, B. Abbas, O. Jucknischke, J. Allgaier, and D. Richter, *Phys. Rev. Lett.* **80**, 4450 (1998).
- ²⁹A. Jusufi, M. Watzlawek, and H. Löwen, *Macromolecules* **32**, 4470 (1999).
- ³⁰M. Watzlawek, C. N. Likos, and H. Löwen, *Phys. Rev. Lett.* **82**, 5289 (1999).
- ³¹M. Daoud and J. P. Cotton, *J. Phys. (Paris)* **43**, 531 (1982).
- ³²A. A. Louis, P. G. Bolhuis, J.-P. Hansen, and E. J. Meijer, *Phys. Rev. Lett.* **85**, 2522 (2000).
- ³³B. Krüger, L. Schäfer, and A. Baumgärtner, *J. Phys. (Paris)* **50**, 3191 (1989).
- ³⁴P. G. Bolhuis, A. A. Louis, J.-P. Hansen, and E. J. Meijer, *J. Chem. Phys.* **114**, 4296 (2001).
- ³⁵A. Jusufi, J. Dzubiella, C. N. Likos, C. von Ferber, and H. Löwen, *J. Phys.: Condens. Matter* **13**, 6177 (2001).
- ³⁶J. des Cloizeaux, *J. Phys. (Paris)* **41**, 223 (1980).
- ³⁷C. von Ferber, Yu. Holovatch, A. Jusufi, C. N. Likos, H. Löwen, and M. Watzlawek, *J. Mol. Liq.* **93**, 151 (2001).
- ³⁸C. von Ferber, A. Jusufi, M. Watzlawek, C. N. Likos, and H. Löwen, *Phys. Rev. E* **62**, 6949 (2000).
- ³⁹P. Pincus, *Macromolecules* **24**, 2912 (1991).
- ⁴⁰M. Watzlawek, H. Löwen, and C. N. Likos, *J. Phys.: Condens. Matter* **10**, 8189 (1998).
- ⁴¹J. L. Lebowitz and J. S. Rowlinson, *J. Chem. Phys.* **41**, 133 (1964).
- ⁴²T. Biben and J.-P. Hansen, *J. Phys.: Condens. Matter* **3**, F65 (1991).
- ⁴³J. P. Hansen and I. R. McDonald, *Theory of Simple Liquids*, 2nd ed. (Academic, London, 1986).
- ⁴⁴J. L. Lebowitz, *Phys. Rev.* **133**, A895 (1964).
- ⁴⁵N. W. Ashcroft and D. Langreth, *Phys. Rev.* **156**, 685 (1967); **166**, 934(E) (1968).
- ⁴⁶R. J. Baxter, *J. Chem. Phys.* **52**, 4559 (1970).
- ⁴⁷A. B. Bhatia and D. E. Thornton, *Phys. Rev. B* **2**, 3004 (1970).
- ⁴⁸N. F. Carnahan and K. E. Starling, *J. Chem. Phys.* **51**, 635 (1969).
- ⁴⁹A. Lang, C. N. Likos, M. Watzlawek, and H. Löwen, *J. Phys.: Condens. Matter* **12**, 5087 (2000).
- ⁵⁰A. A. Louis, P. G. Bolhuis, and J.-P. Hansen, *Phys. Rev. E* **62**, 7961 (2000).
- ⁵¹C. N. Likos, A. Lang, M. Watzlawek, and H. Löwen, *Phys. Rev. E* **63**, 031206 (2001).
- ⁵²J. Dzubiella, H. M. Harreis, C. N. Likos, and H. Löwen, *Phys. Rev. E* **64**, 011405 (2001).
- ⁵³C. N. Likos and H. M. Harreis, *Condens. Matter Phys.* **5**, 173 (2002).
- ⁵⁴I. D'Amico and H. Löwen, *Physica A* **237**, 25 (1997).
- ⁵⁵E. Allahyarov, I. D'Amico, and H. Löwen, *Phys. Rev. Lett.* **81**, 1334 (1998).
- ⁵⁶E. Allahyarov and H. Löwen, *J. Phys.: Condens. Matter* **13**, L277 (2001).
- ⁵⁷A. A. Louis, R. Roth, E. Allahyarov, and H. Löwen, *Phys. Rev. E* (in press).
- ⁵⁸R. Dickman, P. Attard, and V. Simonian, *J. Chem. Phys.* **107**, 205 (1997).
- ⁵⁹M. Dijkstra, R. van Roij, and R. Evans, *Phys. Rev. E* **59**, 5744 (1999).
- ⁶⁰J. M. Méndez-Alcaraz and R. Klein, *Phys. Rev. E* **61**, 4095 (2000).
- ⁶¹A. König and N. W. Ashcroft, *Phys. Rev. E* **63**, 041203 (2001).
- ⁶²P. Attard, *J. Chem. Phys.* **91**, 3083 (1989).
- ⁶³K. R. Hall, *J. Chem. Phys.* **57**, 2252 (1972).
- ⁶⁴J. A. Barker and D. Henderson, *J. Chem. Phys.* **47**, 4714 (1967).
- ⁶⁵L. Verlet and J. J. Weis, *Phys. Rev. A* **5**, 939 (1972).
- ⁶⁶J. M. Kincaid and J. J. Weis, *Mol. Phys.* **34**, 931 (1977).
- ⁶⁷M. H. J. Hagen and D. Frenkel, *J. Chem. Phys.* **101**, 4093 (1994).
- ⁶⁸L. Mederos and G. Navascués, *J. Chem. Phys.* **101**, 9841 (1994).
- ⁶⁹T. Coussaert and M. Baus, *Phys. Rev. E* **52**, 862 (1995).
- ⁷⁰A. Lang, G. Kahl, C. N. Likos, H. Löwen, and M. Watzlawek, *J. Phys.: Condens. Matter* **11**, 10143 (1999).
- ⁷¹S. Melchionna and J. P. Hansen, *Phys. Chem. Chem. Phys.* **2**, 3465 (2000).
- ⁷²D. Goulding and S. Melchionna, *Phys. Rev. E* **64**, 011403 (2001).
- ⁷³R. Roth and R. Evans, *Europhys. Lett.* **53**, 271 (2001).
- ⁷⁴A. A. Louis and R. Roth, *J. Phys.: Condens. Matter* **13**, L777 (2001).
- ⁷⁵A. Johner, J. F. Joanny, S. D. Orrite, and J. B. Avalos, *Europhys. Lett.* **56**, 549 (2001).